ACS APPLIED MATERIALS & INTERFACES

Research Article

Cite This: ACS Appl. Mater. Interfaces 2020, 12, 2871−2877

www.acsami.org

Lattice-Like DNA Tetrahedron Nanostructure as Scaffold to Locate GOx and HRP Enzymes for Highly Efficient Enzyme Cascade Reaction

Ding Wang, Yaqin Chai, Yali Yuan,* and Ruo Yuan*

Key Laboratory of Luminescent and Real-Time Analytical Chemistry (Southwest University), Ministry of Education, College of Chemistry and Chemical Engineering, Southwest University, Chongqing 400715, PR China

Supporting Information

ABSTRACT: In this work, the array arrangement of cascade enzymes was implemented by alternately and equidistantly anchoring two model enzymes glucose oxidase (GOx) and horseradish peroxidase (HRP) to the vertexes of rigid DNA tetrahedron units in lattice-like nucleic acid scaffold, in which the distance between any adjacent cascade enzymes had been regulated to the optimum for obtaining high enzyme cascade catalytic efficiency. Compared to the enzyme cascade system with no-array arrangement of cascade enzymes, the proposed enzyme cascade system allowed the intermediate H_2O_2 produced by GOx catalyzing substrate glucose to concurrently and equidistantly diffuse toward the four adjacent HRP enzyme surfaces. In this case, the invalid diffusion effect of intermediate H_2O_2 between cascade enzymes could be effectively avoided, thereby promoting the enzyme cascade reaction with high catalytic efficiency. The specific catalytic efficiency (k_{cat}/K_m) of the cascade enzyme system with array arrangement had been evaluated, which exhibited catalytic efficiency about 3.6 times higher than that of the randomly arranged cascade enzyme system. As a result, this strategy provided a new avenue for constructing a highly efficient enzyme cascade system with ultimate applications in biosynthesis, bioanalysis, and biodiagnostics.

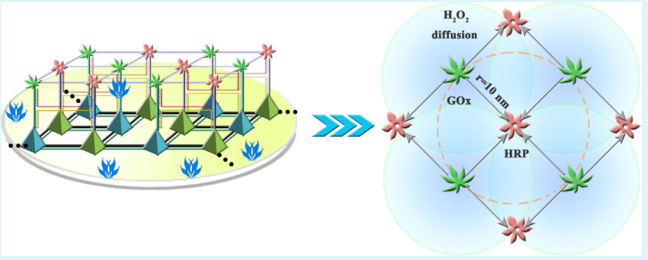

KEYWORDS: *lattice-like DNA tetrahedron nanostructure, DNA self-assembly, enzyme cascade, catalysis, electrochemical biosensor*

INTRODUCTION

In the living system, spatial arrangement for cascade enzymes with natural scaffolds could control the transfer of the intermediates between enzymes from one active site to another, which decreases the invalid diffusion effect and offers a high efficient enzyme cascade reaction.[1−3] Inspired by nature, considerable attention and effort have been devoted to designing artificial scaffolds to arrange cascade enzymes in vitro for various biotechnology applications, including biodiagnostics,[4−6] bioanalysis,[7−9] and biosynthesis.[10,11] Traditional scaffolds, including carbon nanotubes,[12,13] graphene,[14,15] and other support nanomaterials,[16] have been used to coimmobilize cascade enzymes, which enables the local concentration of intermediates to be modulated and facilitates the channelling of intermediates between sequential enzymes. However, in this case, enzymes are usually directly adsorbed or covalently immobilized on these nanomaterial surfaces in a random pattern; here, uncontrolled distribution and location for capture enzymes may largely reduce the catalytic efficiency of the enzyme cascade reaction.[17] Hence, it is critically important to pursuit more reliable scaffold to control the enzymatic distribution and location for high enzyme cascade catalytic efficiency.

Recently, DNA nanostructures emerge as promising scaffolds for arranging molecules at the nanoscale for their sequence-driven, programmable self-assembly.[18−21] For example, cascade enzymes can be positioned on DNA nanostructures with precise control over the spatial distances, with the goals of enhancing the mass transport of intermediates and regulating the catalytic efficiency of enzyme cascade reaction.[22] Some rigid self-assembled DNA nanostructures, including tetrahedron,[23] tweezer,[24,25] and origami,[26] have been utilized as attractive scaffolds to precisely control the arrangement of cascade enzymes for constructing highly efficient enzyme cascade reaction systems. Despite these successes, there are also inevitable defects: the mutual independence between any two scaffolds enables only one or two pairs of cascade enzymes that are simultaneously manipulated by a single scaffold, which could not guarantee the orderly arrangement of all cascade enzymes; thus, some ineffective diffusion of intermediate between cascade enzymes still exists, limiting enzyme cascade catalytic efficiency.

In response, we assume that if these independent DNA scaffolds are assembled together orderly, not only immobilization amount of cascade enzymes can be increased but also the highly ordered arrangement of all cascade enzymes on DNA scaffolds can be achieved, greatly improving the catalytic efficiency of enzyme cascade reaction. Therefore, a lattice-like DNA tetrahedron nanostructure was prepared in our work based on the alternate and equidistant self-assembly of two

Received: October 15, 2019
Accepted: December 18, 2019
Published: December 18, 2019

DOI: 10.1021/acsami.9b18702
ACS Appl. Mater. Interfaces 2020, 12, 2871−2877

types of DNA tetrahedron (TDN) scaffolds decorated with different model enzymes of glucose oxidase (GOx) and horseradish peroxidase (HRP), respectively. Compared with previous DNA scaffolds, the proposed lattice-like nucleic acid scaffold allowed all cascade enzymes in an array arrangement; meanwhile, the distance between any adjacent cascade enzymes was regulated to the optimum, in which the catalytic intermediates produced by any GOx in the array could concurrently diffuse toward four adjacent HRP enzymes surfaces, thus avoiding the invalid diffusion effect of intermediates between cascade enzymes and achieving maximal enzyme cascade catalytic efficiency. Furthermore, the steady-state kinetic data also demonstrated that the cascade enzymes system with array arrangement showed much higher catalytic efficiency than randomly arranged cascade enzyme system. Therefore, this proposed strategy may provide a new ideal for exploring highly efficient enzyme cascade systems with ultimate applications in biodiagnostics, bioanalysis, and biosynthesis.

EXPERIMENTAL SECTION

Materials and Instruments. HRP, $HAuCl_4$, D,L-dithiothreitol, *N*-succinimidyl-3-(2-pyridyldithiol) propionate (SPDP), streptavidin (SA), and GOx were purchased from Sigma (St. Louis, MO, USA). Methylene blue (MB), 3,3′,5,5′-tetramethylbenzidine (TMB), thrombin, glucose, and magnetic nanoparticles (Fe_3O_4NPs) were from Shanghai Aladdin Industrial Corporation (Shanghai, China). Exonuclease I (EXO I) was purchased from New England Biolabs (Beijing, China). The human serum was provided by Third Military Medical University (Chong Qing). All DNA sequences (see Supporting Information in Table S1), purified with high-performance liquid chromatography, were from Sangon Biotech Company, Ltd. (Shanghai, China). Atomic force microscopy (AFM) characterization was performed on Bruker Multimode V8 Scanning Probe Microscopy (USA). The gel image was observed by the Bio-Rad imaging system (Hercules, CA, U.S.A.). All electrochemical data were measured by a CHI 660E electrochemistry workstation (Shanghai Chenhua Instrument, China).

Preparation of TDN-Enzyme Compound. First, two types of single DNA tetrahedron (TDN_1, TDN_2) were synthesized. TDN_1 was assembled by four DNA strands including S_1, S_2, S_3, and S_4. TDN_2 was prepared by the assembly of four DNA strands including S_{10}, S_{20}, S_{30}, and S_{40}. The assembly process was accomplished by mixing equimolar quantities (1 μM) of oligonucleotides in TM buffer (10 mM Tris−HCl, pH 8.0, 1 mM ethylenediaminetetraacetic acid (EDTA), 20 mM $MgCl_2$), then heated to 95 °C for 10 min, and rapidly cooled to 4 °C within 30 s. Specially, here, TDN_1 and TDN_2 separately contained one distinctive thiol-modified pendent probe (a, b) at one vertex and three same pendent probes (c, c′) at the other vertices, in which c pendent in TDN_1 and c′ pendent in TDN_2 were completely complementary to each other. The schematic illustration of designed TDNs is shown in Scheme 1.

Scheme 1. Schematic Illustration of Designed TDN_1 and TDN_2

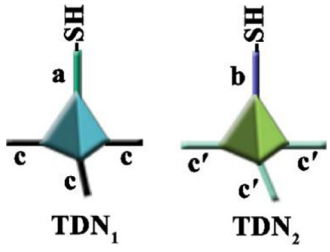

In order to conjugate the enzymes with TDN, a bifunctional coupling linker SPDP was chosen to link thiol-modified pendent probe in TDN and enzymes. First, 100 μL of 5 μM enzyme in phosphate-buffered saline (PBS) buffer (pH 8) was mixed with SPDP (5-fold excess for enzyme) and the mixture reacted at room temperature for 2 h. After excess SPDP was removed by using Amicon 30 kD cutoff filters, the SPDP-modified enzyme was further incubated with 10-fold excess TDN for another 2 h at room temperature. Finally, excess TDN was removed and TDN-enzyme compound was obtained. Based on these procedures, two types of TDN-enzymes including TDN_1-GOx and TDN_2-HRP were prepared and stored at 4 °C for further usage.

Array Arrangement of Cascade Enzymes by Lattice-like Nucleic Acid Scaffold. To form the lattice-like nucleic acid scaffold, prepared free TDN_1-GOx and TDN_2-HRP were casted into the TM buffer containing assisted DNA (AP_1) and cDNA and incubated overnight at 4 °C. In this process, TDN_1 and TDN_2 were alternately assembled to obtain the lattice-like nucleic acid nanostructure; meanwhile, assisted DNA (AP_1) and cDNA could induce the formation of four way DNA junction between any adjacent TDN units, thereby all GOx, HRP on TDN units were alternately and equidistantly located on lattice-like nucleic acid scaffold to realize the array arrangement of cascade enzymes (as shown in Scheme 2).

Polyacrylamide-Gel Electrophoresis. The 8% fresh polyacrylamide gel was prepared with 5× TBE buffer (445 mM Tris, 445 mM boric acid, 10 mM EDTA, pH 8.0). DNA samples mixed with the DNA-loading buffer (volume ratio 5:1) ran at 120 V for 1.5 h in 1× TBE buffer.

AFM Imaging. For AFM imaging, 0.5% (3-aminopropyl)-triethoxysilane (APTES) was dropped onto a freshly cleaved mica surface and incubated for 2 min, then washed by deionized water, and dried by compressed air. After that, 10 μL of the DNA sample (10 nM, diluted with TM buffer) was spotted onto the mica surface and incubated for 5 min at ambient temperature to allow the sample to absorb onto the substrate. Finally, 40 μL of additional TM buffer was added to the liquid cell, and AFM images were observed in fluid mode.

Kinetic Analysis. The kinetic experiment was conducted in a mixture solution containing cascade enzymes GOx/HRP, TMB, and glucose using a UV-2550 UV−vis spectrophotometer (Shimadzu, Tokyo, Japan). The Michaelis constant was calculated by using the following Lineweaver−Burk plot: $1/V = K_m/V_{max}(1/[S] + 1/K_m)$, where V stands for the initial velocity, V_{max} stands for the maximal reaction velocity, and [S] stands for the substrate concentration.

Electrochemical Measurements. Before electrochemical measurements, the cDNA product from Exo I-assisted target recycling reaction was dropped on the prepared biosensor and incubated for 2 h at room temperature. Afterward, the electrode was immersed in 2 mL of PBS buffer (pH 7.0) containing glucose and MB for DPV measurements with the potential from −0.5 to 0.1 V (pulse amplitude of 50 mV, step potential of 4 mV).

RESULTS AND DISCUSSION

Time-Dependent Absorbance Changes toward Different Enzyme Catalytic Systems. Colorimetric assay was used to investigate the occurrence of enzyme cascade system with the introduction of reactant glucose and reporter TMB in detection buffer. In this process, glucose was first catalyzed into gluconic acid by GOx with the concomitant formation of H_2O_2. H_2O_2 was subsequently utilized by HRP to oxidize TMB to produce a blue color, providing maximum absorption peak at 652 nm (see Supporting Information, Figure S1). For comparison, the catalytic efficiency of different enzyme cascade systems was studied. In Figure 1, the cascade enzyme system with array arrangement, cascade enzyme system with no-array arrangement (free cascade enzymes), and blank sample were measured by monitoring the real-time absorbance change. The cascade enzymes system with array arrangement exhibited

DOI: 10.1021/acsami.9b18702
ACS Appl. Mater. Interfaces 2020, 12, 2871−2877

Scheme 2. Array Arrangement of Cascade Enzymes Implemented by Alternate and Equidistant Self-Assembly of Two Types of DNA Tetrahedron Scaffolds Decorated With Different Model Enzymes of GOx and HRP

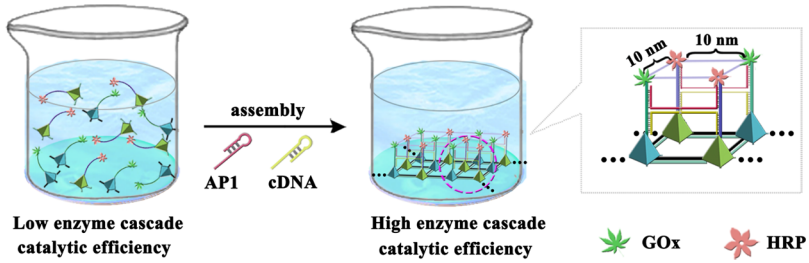

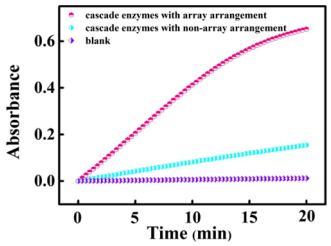

Figure 1. Time-dependent absorbance changes of different cascade enzymes systems, including cascade enzymes with array arrangement, cascade enzymes with no-array arrangement, and blank sample (1 mM TMB as chromogenic agent).

obvious absorbance increase in cascade reaction than that of cascade enzymes system with non-array arrangement and blank control sample, which could be attributed to the fact that the array arrangement of cascade enzymes effectively avoided the invalid diffusion effect of intermediates H_2O_2 between cascade enzymes, thereby promoting the enzyme cascade reaction with high catalytic efficiency.[27−30]

Lineweaver−Burk Plots of Different Cascade Enzymes Systems. To further explore the catalytic efficiency of different cascade enzymes systems with array arrangement and non-array arrangement, the steady-state kinetic parameters were calculated on the basis of the Lineweaver−Burk strategy (Figure 2). The kinetic experiments were performed by fixing one substrate concentration and varying the other substrate concentration. As shown in Figure 2A, for the cascade enzymes system with no-array arrangement (free cascade enzymes), in a certain range of glucose concentration, typical Michaelis−Menten curves were obtained. By fitting the curves with the Michaelis−Menten model (Figure 2B), the corresponding steady-state kinetics parameters were obtained, and the Michaelis constant K_m of the provided cascade enzymes system was 2.96 mM. Meanwhile, for the cascade enzymes system with array arrangement, the typical Michaelis−Menten curve also was obtained for glucose (Figure 2C). The corresponding K_m was 1.42 mM from Figure 2D. For comparison, we could conclude that cascade enzymes system with array arrangement possessed a stronger affinity toward substrate than that of no-array arrangement. In addition, the k_{cat}/K_m values of cascade enzymes system with array arrangement was calculated to be 5.26 s^{-1} mM^{-1}, which was about 3.6 times higher than that of the no-array arrangement (1.47 s^{-1} mM^{-1}), demonstrating an obvious improvement in catalytic efficiency of cascade enzymes system with the array arrangement.

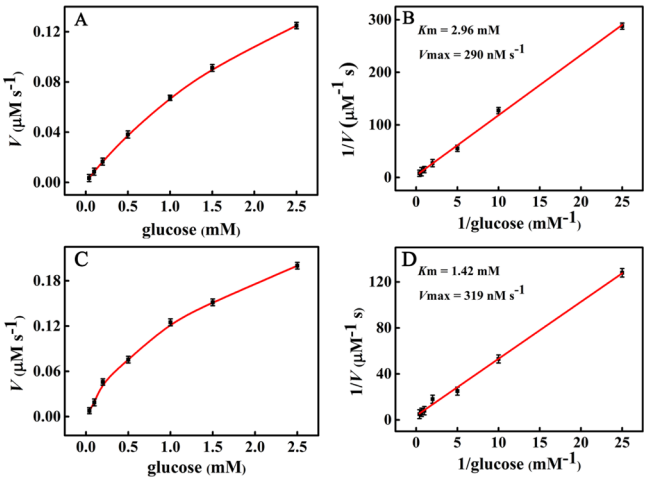

Figure 2. Kinetic assay: (A,C) correlation of initial reaction velocity with the varied glucose concentrations for different cascade enzymes systems with non-array arrangement and array arrangement, respectively. The corresponding double-reciprocal plots (B,D).

Characterization of the Lattice-like DNA Tetrahedron Nanostructure. In this work, for orderly manipulating the array arrangement of cascade enzymes, lattice-like DNA tetrahedron nanostructure as a superior scaffold was prepared based on the successive and alternate assembly of two types of DNA tetrahedron (TDN_1 and TDN_2). To verify the successful preparation of lattice-like nucleic acid scaffold, the polyacrylamide-gel electrophoresis experiment was first performed and the results are shown in Figure 3. In Figure 3A, obvious bands in lanes 1−4 were observed, which corresponded to the single strand DNA of S_1, S_2, S_3, and S_4, respectively. After these four single strands were mixed for DNA self-assembly, a strong band with slow migration than any single strand DNA was noticed in lane 5, suggesting the successful preparation of TDN_1. Similarly, lanes 6−9 represented the single strand DNA (S_{10}, S_{20}, S_{30}, S_{40}), respectively, and the bright band shown in lane 10 stood for the assembly product of TDN_2 unit. Meanwhile, in the other parallel electrophoresis cell, the

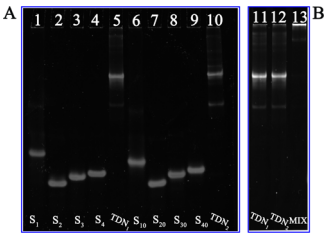

Figure 3. Electrophoresis characterization for the TDN_1, TDN_2 units (A) and lattice-like DNA tetrahedron nanostructure (B).

DOI: 10.1021/acsami.9b18702
ACS Appl. Mater. Interfaces 2020, 12, 2871−2877

assembly procedure of the lattice-like nucleic acid scaffold was validated, and the result is shown in Figure 3B. Here, lane 11 and lane 12 represented the TDN_1 and TDN_2 products, respectively, which were corresponding to the result in Figure 3A. After TDN_1 was incubated with TDN_2 overnight at 4 °C, the mixture product exhibited the slowest migration rate in lane 13, which demonstrated the successful preparation of the lattice-like DNA tetrahedron nanostructure.

The successful formation of lattice-like nucleic acid scaffold also was verified by AFM (Figure 4). Here, obvious lattice-like

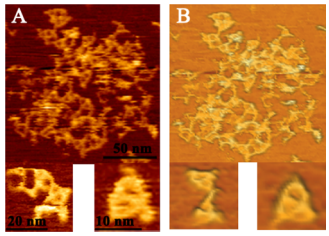

Figure 4. Line profile (A) and 3D view (B) of the AFM images for proposed lattice-like nucleic acid scaffold.

DNA tetrahedron nanostructure is shown in Figure 4A, and the TDN unit also could be seen clearly, suggesting that the lattice-like nucleic acid scaffold was successfully assembled as we expected. Meanwhile, the enlarged images of TDN units are shown in the bottom of Figure 4A. Additionally, Figure 4B showed the corresponding 3D view of AFM images in Figure 4A.

Biosensor Application. Inspired by the high enzyme cascade catalytic efficiency of cascade enzymes system with array arrangement, a novel electrochemical biosensor was designed by utilizing lattice-like nucleic acid scaffold to regulate the distance between any cascade enzymes. As illustrated in Scheme 3, free TDN_1-GOx, TDN_2-HRP and assisted strands AP1, AP2 were first mixed together, then the mixture was dropped on the SA/depAu/GCE surface with incubation at room temperature for 2 h. During this process, TDN_1 and TDN_2 were alternately assembled to obtain the lattice-like nucleic acid nanostructure; meanwhile, AP1 simultaneously hybridized with two pendent probes (a and b) in TDN_1 and TDN_2 under the assistance of AP2 to form a flexible switch, which brought the cascade enzymes GOx, HRP on adjacent TDN units in a closed state. And we named this state as the semioptimal arrangement for cascade enzymes in comparison with the randomly arranged cascade enzymes system. However, in this case, the catalytic efficiency of the enzyme cascade reaction was limited because the distance between adjacent enzymes was not optimal. Afterward, output cDNA converted from target cycling amplification was introduced, which thus initiated the toehold displacement reaction to open the forementioned switch and obtain four-way DNA junction, thereby allowing all GOx, HRP on TDN units alternately and equidistantly locating on lattice-like nucleic acid scaffold and realizing the array arrangement of all cascade enzymes. More importantly, the distance between any adjacent cascade enzymes was controlled to an optimal distance (10 nm);[31−35] in this case, invalid diffusion effect of intermediates between cascade enzymes was avoided and maximal enzyme cascade catalytic efficiency was achieved. By monitoring the change of enzyme cascade catalytic response, target thrombin had been successfully detected.

Validation of Enzyme Cascade Amplification Strategy. In order to demonstrate the occurrence of enzyme cascade reaction in designed electrochemical detection system, different electrochemical responses of biosensor incubated with and without glucose were investigated after electron media MB was introduced into detection buffer. As can be seen in Figure 5A, the biosensor incubated without glucose caused weak electrochemical response. However, after adding glucose in the detection buffer, a significant enhancement was produced in electrochemical signal, which was attributed to the occurrence of enzyme cascade catalytic reaction. In this

Scheme 3. Schematic Diagrams of Proposed Electrochemical Biosensor for Target Thrombin Determination: (A) Exo I-Assisted Target Cycling Amplification Strategy; (B) Fabrication Process of Electrochemical Biosensor Based on Target-Triggered Enzyme Cascade Electrocatalysis; (C) Enzyme Cascade Electrocatalytic Process in Detection System

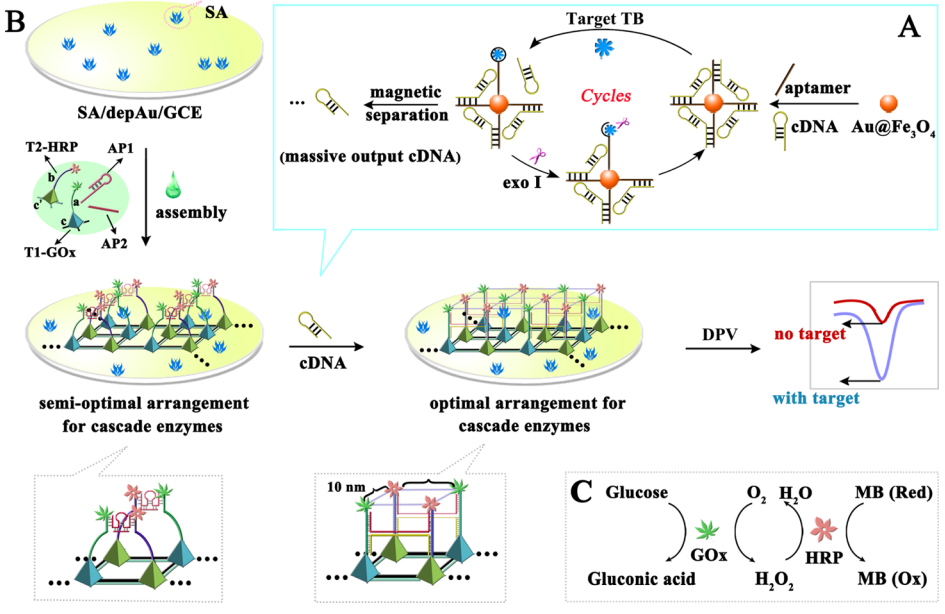

DOI: 10.1021/acsami.9b18702
ACS Appl. Mater. Interfaces 2020, 12, 2871−2877

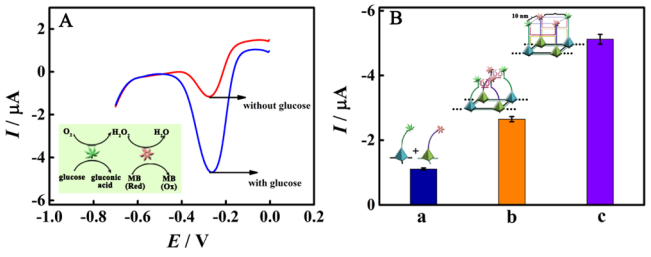

Figure 5. (A) DPV responses of biosensor without and with 4 mM glucose in the PBS detection buffer containing 5 μM MB; (B) DPV responses of biosensor incubated with cascade enzymes under different states, including random arrangement for cascade enzymes (a); semioptimal arrangement for cascade enzymes (b) and optimal arrangement for cascade enzymes (c).

process, glucose in the detection buffer was first oxidized by GOx to yield H_2O_2, then the resulting H_2O_2 was further utilized by HRP to accelerate the oxidation of MB with amplified electrochemical responses.

To further explore the enzyme cascade reaction on modified electrode surface, a series of control experiments were performed, and the results are displayed in Figure 5B. First, when the TDN_1-GOx and TDN_2-HRP were randomly modified on an electrode surface, a low electrochemical response (a) was obtained because uncontrolled distribution and orientation of cascaded enzymes on TDN may largely limit the catalytic efficiency of the enzyme cascade reaction. In comparison with randomly arranged cascade enzymes, the cascade enzymes system with semioptimal arrangement by lattice-like nucleic acid scaffold showed an increase in electrochemical catalytic response, which was ascribed to the fact that lattice-like nucleic acid scaffold enabled cascaded enzymes on TDN units under a relatively controlled condition, thereby decreasing some diffusion effect than random enzymatic arrangement. What is more, the array arrangement of cascade enzymes on lattice-like nucleic acid scaffold resulted in a highest enzyme cascade catalytic response, we could conclude that the intermediates produced by any GOx in the array could concurrently diffuse toward four adjacent HRP enzymes surfaces, thus avoiding invalid diffusion effect of intermediates between cascade enzymes and improving enzyme cascade catalytic efficiency.

Analytical Performance of Thrombin Detection. Under the optimal experimental conditions (see Supporting Information, Figure S3), the performance of the proposed biosensor was assessed by detecting different concentrations of thrombin. It can be seen from Figure 6A that, with the concentration of target thrombin increasing from 1 pM to 10 nM, the DPV current response increased gradually. In addition, a good linear relationship between the DPV current response and thrombin concentrations was obtained (Figure 6B). The linear regression equation was $I = -0.621 \lg c_{target} - 4.215$ with a correlation coefficient of 0.9901. The corresponding detection limit (3σ) is 0.32 pM. Moreover, compared with previously reported electrochemical methods for thrombin assay, our strategy exhibited a wider linear range and a lower LOD (see Supporting Information, Table S2), which could be attributed to the application of highly effective enzyme-assisted target recycling amplification strategy in the cascade enzyme system.

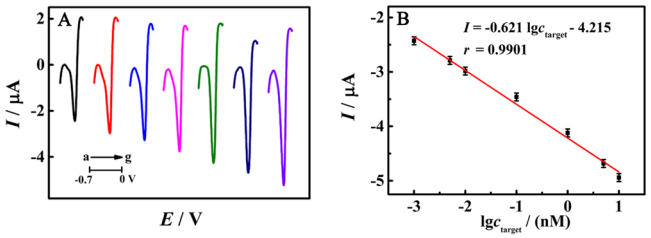

Figure 6. (A) Responses of DPV current to different concentrations of thrombin from 1 pM to 10 nM. (B) Relationship between the current response and the logarithm values of thrombin concentrations.

Reproducibility, Stability, and Specificity of the Biosensor. The reproducibility of the proposed biosensor was explored by measuring five modified electrodes that incubated with the same concentration of thrombin (1 nM) under the same conditions. The relative standard deviation (RSD) of current responses was calculated to be 3.2%, giving a satisfactory reproducibility. The stability of the biosensor was tested via storing it in the fridge at 4 °C and measuring every 5 days. After 10 days, about 96.2% of its original response still retained, which indicated an excellent stability.

Furthermore, four kinds of interfering substances with the same concentration of 1 nM, including Hb, CEA, PSA, and IgG, have been used to evaluate the specificity of the proposed biosensor. The results are shown in Figure 7, and these interferents even with higher concentration (100-fold, 100 nM) than thrombin (1.0 nM) still exhibited feeble current response. Meanwhile, when 1.0 nM thrombin was mixed with the aforementioned four interfering proteins, no apparent signal change existed in comparison with the case of only thrombin. These results suggested the proposed biosensor with excellent specificity for target detection.

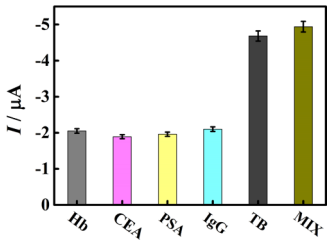

Figure 7. Specificity investigation of proposed biosensor for thrombin (1.0 nM) against other proteins including Hb (100 nM), CEA (100 nM), PSA (100 nM), and IgG (100 nM).

CONCLUSIONS

In summary, a lattice-like tetrahedron nanostructure was prepared by alternate and equidistant self-assembly of two types of DNA tetrahedron (TDN) decorated with different model enzymes of GOx and HRP to achieve the array arrangement of all cascade enzymes. Under this circumstance, the proposed enzyme cascade system enabled intermediates produced by any GOx catalyzing substrate glucose concurrently diffuse toward four adjacent HRP enzymes surfaces, thus avoiding invalid diffusion effect of intermediates between cascade enzymes and exhibiting much higher catalytic efficiency than that of randomly arranged cascade enzyme system. As a proof of concept, the array arrangement of cascade enzymes with high cascade catalytic efficiency was further applied in the construction of a sensitive electro-

DOI: 10.1021/acsami.9b18702
ACS Appl. Mater. Interfaces 2020, 12, 2871−2877

chemical detection platform for biomarker thrombin detection, which also provided a promising strategy for ultrasensitive monitoring of other biomolecules in sensing analysis and disease diagnosis.

■ ASSOCIATED CONTENT

Supporting Information

The Supporting Information is available free of charge at https://pubs.acs.org/doi/10.1021/acsami.9b18702.

Experimental details for the used oligonucleotides, enzyme-assisted target recycling amplification in biosensor part, biosensor fabrication, electrochemical measurements, characterization of prepared biosensor, and experimental conditions optimization for prepared biosensor and recovery test (PDF)

■ AUTHOR INFORMATION

Corresponding Authors

*E-mail: y198688@swu.edu.cn. Phone: +86-23-68252277. Fax: +86-23-68253172 (Y.Y.).
*E-mail: yuanruo@swu.edu.cn (R.Y.).

ORCID

Yaqin Chai: 0000-0003-4392-9592
Ruo Yuan: 0000-0003-3664-6236

Notes

The authors declare no competing financial interest.

■ ACKNOWLEDGMENTS

This work was financially supported by the NNSF of China (21775124, 21505107, 21675129, 21575116), the Fundamental Research Funds for the Central Universities (SWU115037, XDJK2019B022), the Chongqing Research Program of Basic Research and Frontier Technology (cstc2018jcyjA0797).

■ REFERENCES

(1) Chen, Y.; Ke, G.; Ma, Y.; Zhu, Z.; Liu, M.; Liu, Y.; Yan, H.; Yang, C. J. A Synthetic Light-Driven Substrate Channeling System for Precise Regulation of Enzyme Cascade Activity Based on DNA Origami. *J. Am. Chem. Soc.* **2018**, *140*, 8990−8996.

(2) Xia, L.; Van Nguyen, K.; Holade, Y.; Han, H.; Dooley, K.; Atanassov, P.; Banta, S.; Minteer, S. D. Improving the Performance of Methanol Biofuel Cells Utilizing an Enzyme Cascade Bioanode with DNA-Bridged Substrate Channeling. *ACS Energy Lett.* **2017**, *2*, 1435−1438.

(3) Ulyanova, Y.; Arugula, M. A.; Rasmussen, M.; Pinchon, E.; Lindstrom, U.; Singhal, S.; Minteer, S. D. Bioelectrocatalytic Oxidation of Alkanes in a JP-8 Enzymatic Biofuel Cell. *ACS Catal.* **2014**, *4*, 4289−4294.

(4) Chado, G. R.; Stoykovich, M. P.; Kaar, J. L. Role of Dimension and Spatial Arrangement on the Activity of Biocatalytic Cascade Reactions on Scaffolds. *ACS Catal.* **2016**, *6*, 5161−5169.

(5) Moehlenbrock, M. J.; Toby, T. K.; Waheed, A.; Minteer, S. D. Metabolon Catalyzed Pyruvate/Air Biofuel Cell. *J. Am. Chem. Soc.* **2010**, *132*, 6288−6289.

(6) Wei, T.; Du, D.; Zhu, M.-J.; Lin, Y.; Dai, Z. An Improved Ultrasensitive Enzyme-Linked Immunosorbent Assay Using Hydrangea-Like Antibody-Enzyme-Inorganic Three-in-One Nanocomposites. *ACS Appl. Mater. Interfaces* **2016**, *8*, 6329−6335.

(7) Kou, B.; Chai, Y.; Yuan, Y.; Yuan, R. Dynamical Regulation of Enzyme Cascade Amplification by a Regenerated DNA Nanotweezer for Ultrasensitive Electrochemical DNA Detection. *Anal. Chem.* **2018**, *90*, 10701−10706.

(8) Xing, C.; Huang, Y.; Dai, J.; Zhong, L.; Wang, H.; Lin, Y.; Li, J.; Lu, C.-H.; Yang, H.-H. Spatial Regulation of Biomolecular Interactions with a Switchable Trident-Shaped DNA Nanoactuator. *ACS Appl. Mater. Interfaces* **2018**, *10*, 32579−32587.

(9) Zhu, C.; Yang, G.; Li, H.; Du, D.; Lin, Y. Electrochemical Sensors and Biosensors Based on Nanomaterials and Nanostructures. *Anal. Chem.* **2015**, *87*, 230−249.

(10) Dueber, J. E.; Wu, G. C.; Malmirchegini, G. R.; Moon, T. S.; Petzold, C. J.; Ullal, A. V.; Prather, K. L. J.; Keasling, J. D. Synthetic Protein Scaffolds Provide Modular Control over Metabolic Flux. *Nat. Biotechnol.* **2009**, *27*, 753−759.

(11) Conrado, R. J.; Wu, G. C.; Boock, J. T.; Xu, H.; Chen, S. Y.; Lebar, T.; Turnšek, J.; Tomšič, N.; Avbelj, M.; Gaber, R.; Koprivnjak, T.; Mori, J.; Glavnik, V.; Vovk, I.; Benčina, M.; Hodnik, V.; Anderluh, G.; Dueber, J. E.; Jerala, R.; DeLisa, M. P. DNA-guided Assembly of Biosynthetic Pathways Promotes Improved Catalytic Efficiency. *Nucleic Acids Res.* **2012**, *40*, 1879−1889.

(12) Eguílaz, M.; Villalonga, R.; Yáñez-Sedeño, P.; Pingarrón, J. M. Designing Electrochemical Interfaces with Functionalized Magnetic Nanoparticles and Wrapped Carbon Nanotubes as Platforms for the Construction of High-Performance Bienzyme Biosensors. *Anal. Chem.* **2011**, *83*, 7807−7814.

(13) Fu, Y.; Zeng, D.; Chao, J.; Jin, Y.; Zhang, Z.; Liu, H.; Li, D.; Ma, H.; Huang, Q.; Gothelf, K. V.; Fan, C. Single-Step Rapid Assembly of DNA Origami Nanostructures for Addressable Nanoscale Bioreactors. *J. Am. Chem. Soc.* **2013**, *135*, 696−702.

(14) Hu, W.; Peng, C.; Luo, W.; Lv, M.; Li, X.; Li, D.; Huang, Q.; Fan, C. Graphene-Based Antibacterial Paper. *ACS Nano* **2010**, *4*, 4317−4323.

(15) He, S.; Song, B.; Li, D.; Zhu, C.; Qi, W.; Wen, Y.; Wang, L.; Song, S.; Fang, H.; Fan, C. A Graphene Nanoprobe for Rapid, Sensitive, and Multicolor Fluorescent DNA Analysis. *Adv. Funct. Mater.* **2010**, *20*, 453−459.

(16) Mazur, M.; Barras, A.; Kuncser, V.; Galatanu, A.; Zaitzev, V.; Turcheniuk, K. V.; Woisel, P.; Lyskawa, J.; Laure, W.; Siriwardena, A.; Boukherroub, R.; Szunerits, S. Iron Oxide Magnetic Nanoparticles with Versatile Surface Functions Based on Dopamine Anchors. *Nanoscale* **2013**, *5*, 2692−2702.

(17) Zhang, Y.; Hess, H. Toward Rational Design of High-efficiency Enzyme Cascades. *ACS Catal.* **2017**, *7*, 6018−6027.

(18) He, L.; Lu, D.-Q.; Liang, H.; Xie, S.; Luo, C.; Hu, M.; Xu, L.; Zhang, X.; Tan, W. Fluorescence Resonance Energy Transfer-Based DNA Tetrahedron Nanotweezer for Highly Reliable Detection of Tumor-Related mRNA in Living Cells. *ACS Nano* **2017**, *11*, 4060−4066.

(19) Wu, Z.; Liu, G.-Q.; Yang, X.-L.; Jiang, J.-H. Electrostatic Nucleic Acid Nanoassembly Enables Hybridization Chain Reaction in Living Cells for Ultrasensitive mRNA Imaging. *J. Am. Chem. Soc.* **2015**, *137*, 6829−6836.

(20) Zhou, H.; Liu, J.; Xu, J.-J.; Chen, H.-Y. Highly Sensitive Electrochemiluminescence Detection of Single-Nucleotide Polymorphisms Based on Isothermal Cycle-Assisted Triple-Stem Probe with Dual-Nanoparticle Label. *Anal. Chem.* **2011**, *83*, 8320−8328.

(21) Ge, L.; Sun, X.; Hong, Q.; Li, F. Ratiometric NanoCluster Beacon: A Label-Free and Sensitive Fluorescent DNA Detection Platform. *ACS Appl. Mater. Interfaces* **2017**, *9*, 13102−13110.

(22) Fu, J.; Yang, Y. R.; Dhakal, S.; Zhao, Z.; Liu, M.; Zhang, T.; Walter, N. G.; Yan, H. Assembly of Multienzyme Complexes on DNA Nanostructures. *Nat. Protoc.* **2016**, *11*, 2243−2273.

(23) Wang, D.; Chai, Y.; Yuan, Y.; Yuan, R. Precise Regulation of Enzyme Cascade Catalytic Efficiency with DNA Tetrahedron as Scaffold for Ultrasensitive Electrochemical Detection of DNA. *Anal. Chem.* **2019**, *91*, 3561−3566.

(24) Xin, L.; Zhou, C.; Yang, Z.; Liu, D. Regulation of an Enzyme Cascade Reaction by a DNA Machine. *Small* **2013**, *9*, 3088−3091.

(25) Liu, M.; Fu, J. L.; Hejesen, C.; Yang, Y. H.; Woodbury, N. W.; Gothelf, K.; Liu, Y.; Yan, H. A DNA Tweezer-actuated Enzyme Nanoreactor. *Nat. Commun.* **2013**, *4*, 2127.

(26) Ke, G.; Liu, M.; Jiang, S.; Qi, X.; Yang, Y. R.; Wootten, S.; Zhang, F.; Zhu, Z.; Liu, Y.; Yang, C. J.; Yan, H. Directional Regulation of Enzyme Pathways through the Control of Substrate Channeling on

DOI: 10.1021/acsami.9b18702
ACS Appl. Mater. Interfaces 2020, 12, 2871−2877

a DNA Origami Scaffold. *Angew. Chem., Int. Ed.* **2016**, *55*, 7483−7486.
(27) Küchler, A.; Yoshimoto, M.; Luginbühl, S.; Mavelli, F.; Walde, P. Enzymatic Reactions in Confined Environments. *Nat. Nanotechnol.* **2016**, *11*, 409−420.
(28) Zhang, Y.; Tsitkov, S.; Hess, H. Complex Dynamics in a Two-enzyme Reaction Network with Substrate Competition. *Nat. Catal.* **2018**, *1*, 276−281.
(29) Kong, L.; Wang, D.; Chai, Y.; Yuan, Y.; Yuan, R. Electrocatalytic Efficiency Regulation between Target-Induced HRP-Mimicking DNAzyme and GOx with Low Background for Ultrasensitive Detection of Thrombin. *Anal. Chem.* **2019**, *91*, 10289−10294.
(30) Yang, Y. R.; Liu, Y.; Yan, H. DNA Nanostructures as Programmable Biomolecular Scaffolds. *Bioconjugate Chem.* **2015**, *26*, 1381−1395.
(31) Ngo, T. A.; Nakata, E.; Saimura, M.; Morii, T. Spatially Organized Enzymes Drive Cofactor-Coupled Cascade Reactions. *J. Am. Chem. Soc.* **2016**, *138*, 3012−3021.
(32) Kou, B.-B.; Chai, Y.-Q.; Yuan, Y.-L.; Yuan, R. PtNPs as Scaffolds to Regulate Interenzyme Distance for Construction of Efficient Enzyme Cascade Amplification for Ultrasensitive Electrochemical Detection of MMP-2. *Anal. Chem.* **2017**, *89*, 9383−9387.
(33) Zhang, Y.; Hess, H. Toward Rational Design of High-efficiency Enzyme Cascades. *ACS Catal.* **2017**, *7*, 6018−6027.
(34) Wang, D.; Chai, Y.; Yuan, Y.; Yuan, R. Precise Regulation of Enzyme Cascade Catalytic Efficiency with DNA Tetrahedron as Scaffold for Ultrasensitive Electrochemical Detection of DNA. *Anal. Chem.* **2019**, *91*, 3561−3566.
(35) Fu, J.; Liu, M.; Liu, Y.; Woodbury, N. W.; Yan, H. Interenzyme Substrate Diffusion for an Enzyme Cascade Organized on Spatially Addressable DNA Nanostructures. *J. Am. Chem. Soc.* **2012**, *134*, 5516−5519.

DOI: 10.1021/acsami.9b18702
ACS Appl. Mater. Interfaces 2020, 12, 2871−2877